DESIGNED MONOMERS AND POLYMERS
2020, VOL. 23, NO. 1, 197–206
https://doi.org/10.1080/15685551.2020.1837442

Preparation of amphiphilic magnetic polyvinyl alcohol targeted drug carrier and drug delivery research

Yazhen Wang[a,b,c], Zhen Shi[a,b], Yu Sun[b], Xueying Wu[b], Shuang Li[b], Shaobo Dong[b] and Tianyu Lan[b]

[a]College of Materials Science and Engineering, Qiqihar University, Qiqihar, China; [b]Heilongjiang Provincial Key Laboratory of Polymeric Composite Materials, Qiqihar, China; [c]College of Chemistry, Chemical Engineering and Resource Utilization, Northeast Forestry University, Harbin, China

ABSTRACT

Currently, magnetic applications have great potential for development in the field of drug carriers. In this paper, Fe_3O_4-PVA@SH, an amphiphilic magnetically targeting drug carrier, was prepared by using Fe_3O_4 and PVA with thiohydrazide-iminopropyltriethoxysilane(TIPTS). The loading capacity of Fe_3O_4-PVA@SH on Aspirin and the drug release kinetics of loaded drugs were studied. The obtained Fe_3O_4-PVA@SH exhibits excellent drug release properties in simulating the human body fluid environment (pH 7.2). Since magnetically targeting drug carriers are readily available and have excellent biocompatibility and the characteristics of drug release. This work's development, preparing amphiphilic magnetically targeting drug carriers in drug delivery and other fields, has great significance.

ARTICLE HISTORY
Received 2 September 2020
Accepted 12 October 2020

KEYWORDS
Fe_3O_4; magnetic; Poly(vinyl alcohol); targeted drug delivery; amphiphilic

1. Introduction

Nanotechnology helps develop new pharmaceutical agents, drug delivery, and the synthesis of drug carriers [1–3]. Playing a vital role in treating human diseases (such as malignant tumors and heart disease) by using magnetic cores to target therapeutic drugs. [4–7] Recently, efforts include targeted delivery. Drugs are only active in specific areas of the body (such as cancerous areas or lesions), and medications can be released in a controlled manner over a while [8–12]. Magnetic nanoparticles are a carrier form used for targeted therapy, with a particle size between 1 ~ 100 nm. The magnetic nanoparticles concentrate the drug carrier in the target region through the magnetic field. The drug can be released smoothly, increase the target's concentration, enhance the therapeutic effect, reduce the distribution in other parts, and reduce toxicity and side effects. The drug carrier controls the release of the drug to have an excellent therapeutic effect. The loading and releasing of drugs must be performed [13–16].The core part of the magnetically targeting drug carrier is iron oxide nanoparticles due to the superparamagnetic and single domain characteristics of iron oxide nanoparticles [17–21].The target is provided by a magnetic polymer made of Fe_3O_4 as a magnetic core and is coated with the magnetic polymer. The polymer's purpose is to make Fe_3O_4 nanoparticles as a magnetic core to be better and more uniformly distributed in the drug carrier. When Fe_3O_4 nanoparticles are coated with high molecular polymers, they can be used in drug carriers. Superparamagnetic iron oxide was used extensively in the detection of atherosclerotic plaque. And expanded-pore nanoparticles functionalized with N-isopropyl acrylamide and poly(ethylene glycol) were applied for temperature control release of bovine hemoglobin. Compared with small molecule drugs with passive targeting, polymer-drug carriers generally exhibit better pharmacokinetics. [22–26]

In the drug carrier's actual application, the targeted drug carrier should have good biocompatibility and accurately target the body fluid environment's desired location [27,28].As a magnetic material, Fe_3O_4 is widely used in human treatment because of its stable quality, superparamagnetic properties, and easy realization. Fe_3O_4 nanoparticles are widely used as biomaterials and exhibit superparamagnetic properties in magnetic resonance imaging (MRI), targeted hyperthermia, drug delivery, and immobilized proteins [29–33].However, as a magnetically targeting drug carrier, its biocompatibility is poor. A variety of natural and synthetic biodegradable polymers are used for drug delivery [34–36].Among various polymers, polyvinyl alcohol (PVA) has received more and more attention. It is a biodegradable, biocompatible, water-soluble, and inexpensive polymer [37–40].It has good water solubility, good film-forming properties, adhesion, emulsification, and good solvent resistance

CONTACT Yazhen Wang wyz6166@qqhru.edu.cn College of Materials Science and Engineering, Qiqihar University, Qiqihar 161006, China

because PVA molecules have more hydroxyl groups [41–45].Pharmacological experiments have proved that PVA is non-toxic, tasteless, non-irritating to the skin, and will not cause skin allergies. It has been widely used as a drug carrier. When PVA is used in a drug carrier, it exhibits sustained-release properties due to its macromolecular swelling properties. Sustained-release drugs can reduce dosing frequency and improve patients' compliance, especially children and elderly patients [46–49].

Suppose the magnetical drug carriers want to show excellent biocompatibility. In that case, it needs to improve the solubility of the water of their carriers and improve their solubility of lipids. The feature of this study is to improve the lipid solubility of drug carriers through thiohydrazide-iminopropyltriethoxysilane (TIPTS). TIPTS is not only playing a coupling role in the polymerization reaction but also improve the lipid solubility. Good biocompatibility requires good amphiphilic [50,51]. The thiolated polymer and the cysteine-rich(Cys) thiol group in the Cys subdomain of the mucosal glycoprotein form a disulfide bond has strong adhesion and good cohesion [52–56].

Aspirin (acetylsalicylic acid), with a chemical formula $C_9H_8O_4$, is a widely used medicine. Aspirin is a cyclooxygenase (COX) inhibitor. It mainly reduces the synthesis of thromboxane (TXA2) by inhibiting COX activity, thus preventing platelet aggregation and blood clotting. [57–61] Aspirin is also used to prevent first heart attacks.

In this project, Fe_3O_4 is used as a magnetically targeted magnetic carrier. They were improving the water solubility of Fe_3O_4 by the reaction of Fe_3O_4 and PVA to get the Fe_3O_4-PVA. At the same time, the swelling characteristics of PVA makes the entire drug carrier exhibit slow-release characteristics. The Fe_3O_4-PVA reacts with thiohydrazide-aminopropyltriethoxysilane (TIPTS) to synthesize Fe_3O_4-PVA @ SH improving the fat solubility of the drug carrier. On the other hand, the hydroxyl group on Aspirin can form a hydrogen bond(-OH) with the hydroxyl group (-OH) and thiol group(-SH) on Fe_3O_4-PVA @ SH and is loaded on the Fe_3O_4-PVA @ SH carrier, which is transported to the lesion site by the carrier and exerts efficacy. The mechanism is shown in scheme 1.

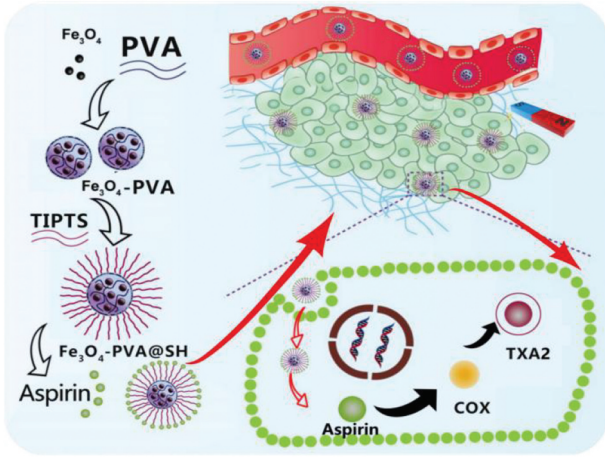

Scheme 1. Schematic illustration of the synthetic route of Fe_3O_4-PVA@SH and the proposed synergistic antithrombotic mechanism of Fe_3O_4-PVA@SH.

2. Experimental section

2.1. Materials

Poly(vinyl alcohol) (PVA) (Mw 4505 (degree of alcoholysis) 87.0–89.0 mol%, viscosity 80.0–110.0 mpa.s), Aspirin (acetylsalicylic acid), Iron(II) chloride tetrahydrate ($FeCl_2 \cdot 4H_2O$), iron(III) chloride hexahydrate($FeCl_3 \cdot 6H_2O$), [55] ammonia solution (25 wt%) were purchased from Aladdin Chemistry Co. Ltd. (Shanghai, China). Dimethyl sulfoxide (DMSO) was purchased from Sinopharm Chemical Reagent Co., Ltd (Shanghai, China). Concentrated sulfuric acid (H_2SO_4) was purchased from Acros Organics (Beijing, China). thiohydrazide-iminopropyltrithoxy-silane (TIPTS) [55], homemade.

2.2. Synthesis of magnetic (Fe_3O_4) nanoparticles [62]

$FeCl_3 \cdot 6H_2O$ (4 g) and $FeCl_2 \cdot 4H_2O$ (2 g) were dissolved in 100 mL of distilled water. The solution ultrasound for an hour. Then, 30 mL of ammonia (NH_3) was added to the solution and stirred for five hours at 70°C. The entire reaction system was carried out under nitrogen protection. Finally, the product was rinsed repeatedly, rinsed with water, and freeze-dried.

2.3. Synthesis of Fe_3O_4-PVA [62]

PVA (3 g) was dissolved in 100 mL of distilled water and stirred using a mechanical stirrer to dissolve. Fe_3O_4 (3 g) was ultrasound for an hour and add it in the PVA solution; the ammonia solution was added to adjust the pH appropriately. The entire reaction system was reacted for 5 h under the protection of nitrogen. The black product was washed with distilled water. Until the solution as the whole system reached a neutral pH, and the samples were freeze-dried.

2.4. Synthesis of Fe_3O_4-PVA@SH

The thiol coupling agent(4 g) and Fe_3O_4-PVA(1 g) were dispersed into 100 mL of DMSO. The solution ultrasound

for 2 h and add H_2SO_4 until the solution system's pH is 1 to 2.Then the entire reaction system was stirred at 35°C for 2 h. Also, the product was centrifuged, rinsed with water, and freeze-drying. At this point, we get Fe_3O_4-PVA @SH. The experimental process is shown in Figure 1.

2.5. Characterization

X-ray powder diffraction (XRD) spectra were taken on a Holland PANalytical X– Pert PRO X-ray diffractometer with Cu–Kα radiation. Fourier transforms infrared (FTIR) spectra were performed on the IRAffinity-1 spectrometer. Infrared spectrum analysis. Scanning electron microscopy (SEM)and Energy Dispersive Spectrometer (EDS) images were recorded using the JSM-6380 LV microscope. Contact angle measuring instrument (JC2000D1, Shanghai). Differential scanning calorimetry (DSC) was carried on a NETZSCH STA 449 C analyzer with a heating rate of 20 °C min^{-1} in nitrogen flow.

2.5.1. Swelling measurements

The swelling properties of the Fe_3O_4-PVA@SH were determined. The swelling ratio was calculated as follows:

$$\text{swellingratio} = (\text{Ws} - \text{Wd})/\text{Wd}$$

Wd and *Ws* are the weight of dried Fe_3O_4-PVA@SH before and after immersing in aqueous solution for 48 h, respectively.

2.5.2. Loading kinetics studies

To investigate the loading kinetics of the Fe_3O_4-PVA@SH for Aspirin, we typically left 45 mg of Fe_3O_4-PVA@SH to soak in 10 mL of an aqueous solution of Aspirin (0.085 mmol/L) at 37°C temperature. After predetermined intervals time, the supernatant solution was collected for analysis by UV spectrophotometer. The amount of Aspirin loaded by Fe_3O_4-PVA@SH the was calculated from the following mass balance equation:

$$Qt = (Co - Ct)/m$$

Qt (mmol/g) is the amount adsorbed per gram of Fe_3O_4-PVA@SH at time *t, Co* is the initial concentration of Aspirin in the solution (mmol/L), *Ct* is the concentration of Aspirin at time *t* (mmol/L), *V* is the volume of the solution (L), and *m* is the mass of the Fe_3O_4-PVA@SH used(g).

2.5.3. Drug release from Fe_3O_4-PVA@SH

For the drug release experiment, the release of Aspirin was determined with a UV–vis spectrophotometer at λmax = 287 nm at a function of time. The typical procedure used as follows: the above aspirin-loaded Fe_3O_4-PVA@SH were kept immersed in 3 mL water of pH = 7.2 at 37°Cand placed on a shaking machine a certain shaking frequency to simulate the process of drug release in the human body. At particular intervals, the supernatant solution was collected for analysis by a UV spectrophotometer. Each experiment was carried out in triplicate.

$$Release = \frac{the amount of aspirin released from Fe_3O_4-PVA@SH}{the total amount of aspirin loaded by Fe_3O_4-PVA@SH} \times 100\%$$

3. Results and discussion

3.1. XRD

According to the XRD pattern, Figure 2 shows the XRD pattern of Fe_3O_4-PVA, TIPTS and Fe_3O_4-PVA@SH nanocomposite. Compared with standard cards. We can be seen that the peaks at 2θ = 30.1°, 35.5°, 43.3°, 57.3°, and 62.7° were assigned to the characteristic peaks of Fe_3O_4 (JCPDS card No. 72–2303), demonstrated that Fe_3O_4 particles were successfully formed in the PVA matrix. The peaks at 2θ = 26.6°, 43.4°, 54.8°, 56.6°, and 63.6° are given to the typical carbon peak of TIPTS(JCPDS card No.26–1097) and confirmed the PVA's semicrystalline properties. The XRD patterns of Fe_3O_4 -PVA shows that the synthesis of Fe_3O_4-PVA was successful [63,64]. The XRD pattern of the nanoparticles containing Fe_3O_4-PVA @SH is shown in Figure 2. Comparing the characteristic peaks on the XRD curves of Fe_3O_4-PVA, TIPTS, and Fe_3O_4-PVA @ SH in the figure. Some characteristic peaks of

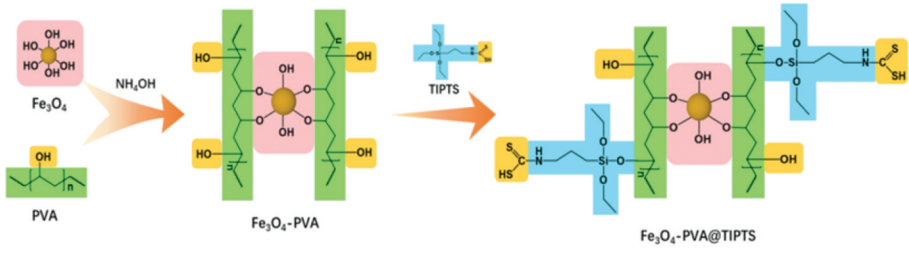

Figure 1. The synthetic route of Fe_3O_4-PVA@SH.

TIPTS have partially deviated. This phenomenon is because that PVA and TIPTS are coated outside Fe_3O_4, which makes the particle size of Fe_3O_4 change massive, the crystal form changes slightly. All shows that PVA and TIPTS are added to the core structure, so this analysis's composite construction is quite evident.

3.2. FT-IR analysis

Infrared spectroscopy was performed to analyze the chemical changes between the incorporated components. The FT-IR spectra of PVA and Fe_3O_4-PVA are shown in Figure 3. The peak seen at 3439 cm^{-1} is attributable to the -OH stretching vibration of PVA. The peak at 2902 cm^{-1} in the infrared spectrum of Fe_3O_4-PVA is due to the stretching vibration of -CH. The peak at 1416 cm^{-1} is due to the stretching vibration of -C-C-, the rise at 1096 cm^{-1} is the stretching vibration peak of Fe-O-C, and the rise at 569 cm^{-1} is due to the stretching vibration of Fe-O- vibration peak. The existence of characteristic peaks indicates that we successfully synthesized Fe_3O_4-PVA. Figure 3 shows the infrared spectra of TIPTS and Fe_3O_4-PVA@SH. The mountain seen in TIPTS at 3435 cm^{-1} is due to the stretching vibration of -OH. The peak at 2583 cm^{-1} in Fe_3O_4-PVA @ SH is -SH, the height at 1432 cm^{-1} is caused by the hydrocarbon bending vibration of $-CH_3$, and the stretching vibration of -CH causes the peak at 2928 cm^{-1}. The height at 1373 cm^{-1} is the typical stretching vibration of -C-C-. The height at 1083 cm^{-1} is the stretching vibration peak of Fe-O-C. The height at 1628 cm^{-1} is the stretching vibration peak -NH, the peak at 798 cm^{-1} is attributed to the stretching vibration peak of Si-O-CH_3. There is no stretching vibration of Fe-O, indicating that Fe_3O_4 is encapsulated to form a magnetic core drug carrier system Fe_3O_4 with thiols and hydroxyl groups. The synthesis of Fe_3O_4-PVA@SH was successful based on the synthesis of Fe-O-C, Si-O-CH_3, and the presence of -SH and -NH, which confirms the formation of Fe_3O_4-PVA@SH.

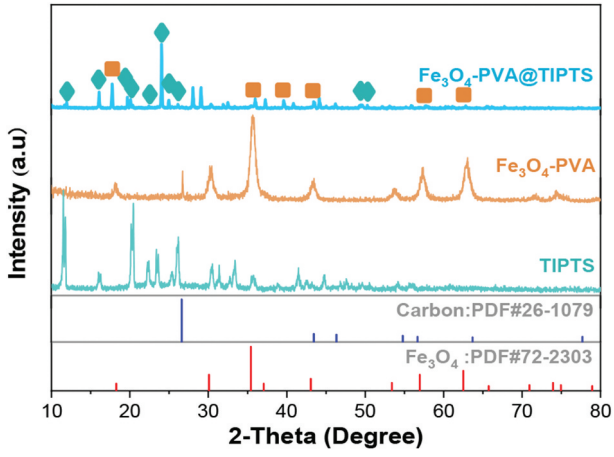

Figure 2. XRD curves of Fe_3O_4-PVA, TIPTS, and Fe_3O_4-PVA@SH.

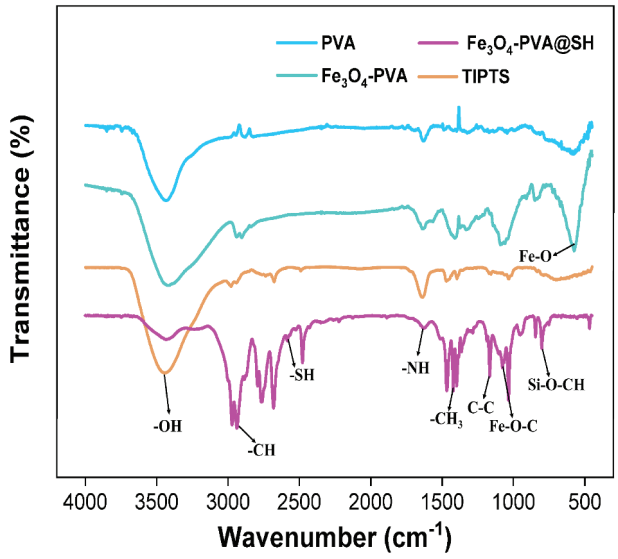

Figure 3. FT-IR spectrum of Fe_3O_4 and Fe_3O_4-PVA, TIPTS, and Fe_3O_4-PVA@SH.

3.3. SEM and EDS

Figure 4(a) shows the SEM images of the Fe_3O_4-PVA synthesized. Accordingly, the synthesis of uniformly distributed spherical structures with a particle diameter of about 60 nm can be seen. Figure 4(d) shows the SEM images of nanoparticles containing Fe_3O_4-PVA @SH with a particle diameter of about 100 nm. Among them, the spherical irregularities are a mixture of PVA and TIPTS. Fe_3O_4 nanoparticles in which the polymeric that cover the core are well visible.

Energy dispersive spectra analysis was performed to the elemental composition of the nanoparticles and confirmed the product's purity Figure 4(b) shows the EDS pattern of Fe_3O_4-PVA. The samples contain C, O, and Fe elements. The elemental analysis obtained from this spectrum indicates that C: O: Fe atomic ratio is 1:1.7:1.1. Figure 4(c) shows the EDS pattern of Fe_3O_4-PVA@SH the samples contain N(Figure 4(e)), C(Figure 4(f)), Fe(Figure 4(g)), Si (Figure 4(h)), O(Figure 4(i)), and S(Figure 4(j)) elements, and that the parts are evenly distributed on the sample.

3.4. Contact angle and nanoparticle size

Figure 5(a) shows the contact angles of Fe_3O_4, Fe_3O_4-PVA and Fe_3O_4-PVA@SH are 91.84 degrees, 54.38 degrees, and 59.32 degrees. Figure 5(b) shows that the particle sizes of Fe_3O_4, Fe_3O_4-PVA, and Fe_3O_4-PVA@SH are 65.17 nm, 74.62 nm, and 88.52 nm, respectively. It has been well documented that the size of less than

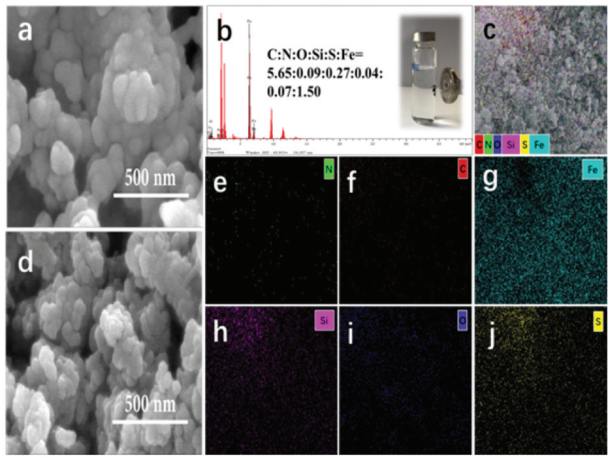

Figure 4. SEM images of (a)Fe_3O_4-PVA and of (d) Fe_3O_4-PVA@SH; (b) EDS images of Fe_3O_4-PVA@SH and Fe_3O_4-PVA@SH magnetic display; (c, e-j)EDS images of Fe_3O_4-PVA@SH.

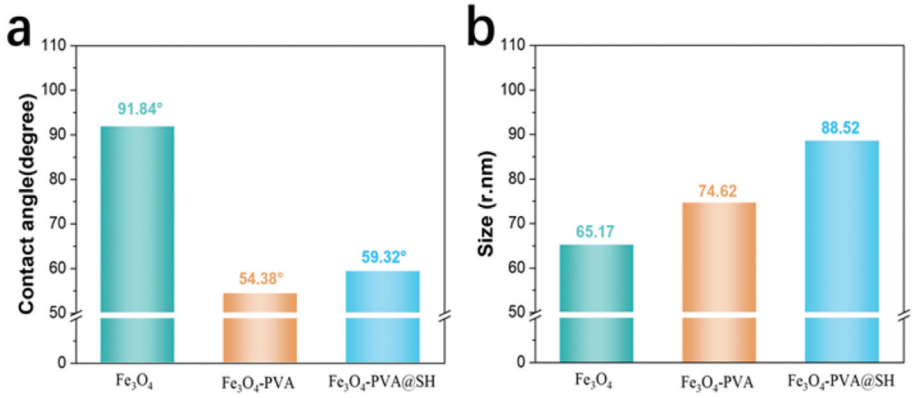

Figure 5. (a)The contact angle histogram shows the changing trend of the contact angle of Fe_3O_4, Fe_3O_4-PVA, and Fe_3O_4-PVA@SH;(b) The particle size histogram shows the changing direction of the contact angle of Fe_3O_4, Fe_3O_4-PVA and Fe_3O_4-PVA@SH.

100 nm is favorable for passive targeting. Fe_3O_4 is coated with polyvinyl alcohol, making Fe_3O_4-PVA have an increased particle size and increased hydrophilicity compared to Fe_3O_4. And Fe_3O_4-PVA@SH is grafted with TIPTS outside, so the particle size of Fe_3O_4-PVA@SH is also slightly increased compared to Fe_3O_4-PVA. And improve the lipid solubility, so the corresponding hydrophilicity has been reduced. Nanoparticle size change again proves the formation of magnetically targeted drug carrier Fe_3O_4-PVA@SH. Respectively, Fe_3O_4 has some hydroxyl groups on the surface, but the number is too small to meet the drug carrier's hydrophilicity requirements. PVA is a hydrophilic polymer. PVA has strong hydrophilicity. PVA has many hydroxyl groups and is coated on Fe_3O_4 to improve the carrier's hydrophilicity. The mercapto group (-SH) is less water-soluble than the hydroxyl group (-OH), so the presence of the mercapto group (-SH) makes the carrier's water solubility slightly lower. At the same time, a suitable drug carrier also needs to have excellent lipophilicity. The thiol group on TIPTS has strong nucleophilicity. The introduction of the thiol group improves the lipid solubility. Improving amphiphilicity allows magnetic targeting drug carriers to have excellent hydrophilicity and lipophilicity, and biological activity is much improved. Moreover, The magnetic targeting drug carrier can form a hydrogen-bonded co-loading drug with the drug, pass through the layers of cells, and target the drug to be transported under the action of an external magnetic field to exert the drug effect and improve the bioavailability.

3.5. VSM

Meanwhile, the magnetic properties of Fe_3O_4, Fe_3O_4-PVA, and Fe_3O_4-PVA@SH were measured by VSM at 300 K (Figure 6) and Table 1. The hysteresis loop shows that Fe_3O_4, Fe_3O_4-PVA, and Fe_3O_4-PVA@SH were superparamagnetic with no coercivity at room

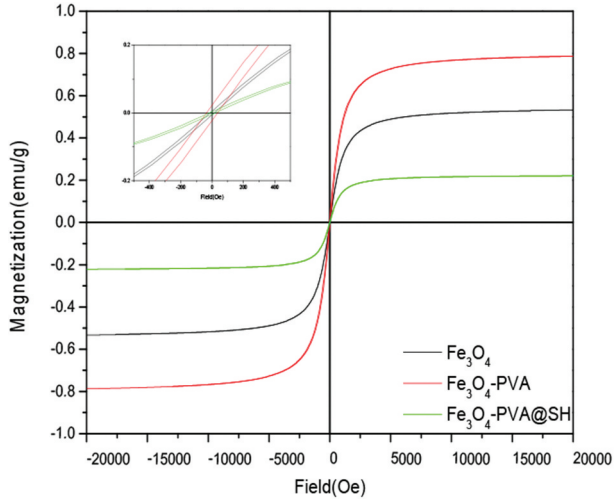

Figure 6. Magnetic hysteresis loops of the Fe_3O_4, Fe_3O_4-PVA, and Fe_3O_4-PVA@SH at 300 K. (The upper left is the detailed picture).

Table 1. The magnetization of Fe_3O_4, Fe_3O_4-PVA, and Fe_3O_4-PVA @SH at 300 K.

Samples	Magnetization(emu/g)
Fe_3O_4	0.78
Fe_3O_4-PVA	0.52
Fe_3O_4-PVA@SH	0.22

temperature. The saturation magnetization values for Fe_3O_4, Fe_3O_4-PVA, and Fe_3O_4-PVA@SH are 0.78emu/g, 0.52emu/g, and 0.22 emu/g, respectively, which means that PVA and TIPTS are wrapped around Fe_3O_4, which further explains Fe_3O_4-PVA@SH preparation was successful. Superparamagnetism of drug carriers is very important for practical applications because, under a particular magnetic field, the drug release performance of Fe_3O_4-PVA@SH may be seriously affected by its magnetic strength [65].

3.6. DSC

Various ingredients of the nanoparticles were also characterized by differential Scanning Calorimeter (DSC) in Figure 7(a) DSC was performed from 60 °C to 450 °C in the N_2 atmosphere with a heating rate of 10°C/min. A degree of about 60 °C to 100 °C there is related to water (moisture) evaporation. At around 100°C to 200 °C, there is a loss regarding side -OH elimination and TIPTS defunctionalization reactions decomposition and 200°C to 330 °C C-C cleavage chain rupture and is decomposed. At a temperature higher than 330°C, residual carbon and Fe_3O_4 has remained.

3.7. Swelling ratio

Also, the swelling ratio of the Fe_3O_4-PVA@SH synthesized at 20°C, 25°C, 30°C, and 35°C was studied, as shown in Figure 7(b). The swelling rates of Fe_3O_4-PVA @ SH synthesized at 20°C, 25°C, 30°C, and 35°C were 148%, 134%, 129%, and 118%, respectively. Also, the stability of the Fe_3O_4-PVA@SH was studied. First, the Fe_3O_4-PVA@SH were immersed in an aqueous solution for 48 h, and then the Fe_3O_4-PVA@SH were separated, and the aqueous residue solution was evaporated and weighed. It is found that all the Fe_3O_4-PVA@SH showed tiny (below 5 wt %) weight loss.

It is well known that the molecular chain structure of the PVA determines the swelling rate, and the reaction temperature can affect the void structure between the molecular chains, thereby affecting the swelling ratio. It can be seen from Figure 7(b) that the swelling ratio is best at 20, and the void structure is more.

3.8. Loading kinetics studies

For drug delivery applications, the drug carrier's loading level is a crucial parameter in practical applications. Here, we choose Aspirin as a model drug to study the loading drug characteristics of the magnetically targeted drug carrier by Fe_3O_4-PVA@SH. The dry Fe_3O_4-PVA@SH was immersed in the aspirin solution for 12 hours to carry out the process of loading aspirin. As shown in Figure 7(c), the loading level of Fe_3O_4-PVA@SH is mainly because the PVA chain can adsorb aspirin molecules through strong interactions (such as van der Waals interactions and hydrogen

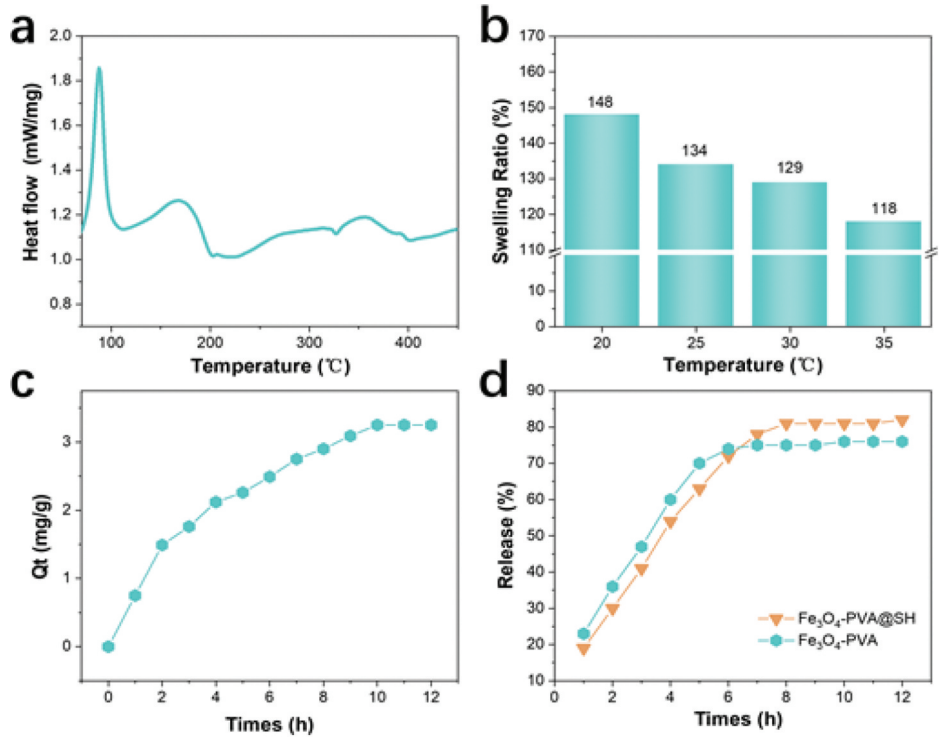

Figure 7. (a) DSC curves of Fe_3O_4-PVA@SH; (b) swelling ratio of Fe_3O_4-PVA@SH synthesized at 20 °C, 25 °C, 30 °Cand35°C; (c) effect of contact time on the and loading amount of Aspirin (0.085 mmol/L, 10 mL) by Fe_3O_4-PVA@SH (45 mg) at 37°C when pH = 7.2; (d) drug release profiles of Fe_3O_4-PVA and Fe_3O_4-PVA@SH at pH 7.2 and 37 temperature.

bonds). There are a lot of sulfhydryls (-SH) groups on TIPTS. Disulfide bonds will be formed between the sulfhydryl polar groups at the end of TIPTS and dispersed between the pores of Fe_3O_4-PVA@SH. For better detection, the drug loading process and drug loading kinetics of Fe_3O_4-PVA @ SH were studied. The effect of contact time on Fe_3O_4-PVA@SH loaded aspirin is shown in Figure 7(c). The initial concentration of Aspirin is 0.085 mmol/L. It can be seen that 50% of Aspirin was loaded in 4 hours, and the sample loading process reached equilibrium in about 10 hours (Figure 7c). Correspondingly, the loading amount of Aspirin on Fe_3O_4-PVA@SH was 2.11 mg/g at 4 h and 3.21 mg/g at 10 h (Figure 7c). We believe that the fast loading rate in the first 4 h is mainly due to Aspirin's adsorption on the outermost layer of Fe_3O_4-PVA@SH. After the outer layer reaches the load balance, the inside of Fe_3O_4-PVA@SH starts to slow down Aspirin's adsorption. Finally, the internal and external adsorption equilibrium is reached.

3.9. Drug release kinetics studies

Because the Fe_3O_4-PVA@SH can load a large number of drugs, it is convenient to investigate their drug release properties in vitro. To investigate the TIPTS study of targeted drug carriers, we compared the drug release profiles of Fe_3O_4-PVA. Two samples, including Fe_3O_4-PVA and Fe_3O_4-PAV@SH chosen and their drug release profiles over time, were presented in Figure 7(d), as observed, significant differences in drug release rates and amount between the two samples. Within 4 h, the release rates of Fe_3O_4-PVA and Fe_3O_4-PVA @ SH are faster, and the release amount of Fe_3O_4-PVA reaches 60% at 4 h, while Fe_3O_4-PAV@ SH is 54%. This phenomenon may be explained as follows: This is due to the rapid release of Aspirin released by the drug carrier's outer layer through strong interactions (van der Waals interaction and hydrogen bonding). The release rate of Fe_3O_4-PVA was gentle at 4 h to 6 h, which was due to the slow release of Aspirin adsorbed by the internal pores of PVA swelling. After 6 h, the release rate of

Fe_3O_4-PVA is almost zero, and the release behavior stops. It can be seen that the drug release rate of Fe_3O_4-PVA @ SH has a slow-release process after 6 h and continues to 8 h. We think that the disulfide bond is formed between the thiol groups of TIPTS, and the disulfide bond break requires more energy than the hydrogen group, which slows the release of Aspirin and makes Fe_3O_4-PVA @SH reach a 3 h slower than Fe_3O_4-PVA release time.

PVA acts as a matrix, and -OH on the PVA chain can form strong interactions with drugs (van der Waals interaction and hydrogen bonding). At the same time, magnetic iron oxide nanoparticles provide targeting for the carrier. TIPTS is used as a biomaterial to improve the lipid solubility of magnetic polyvinyl alcohol. The thiol group on TIPTS can form a disulfide bond internally. It can also include a disulfide bond with the cysteine-rich(Cys) sulfhydryl group in the Cys subdomain of the cell surface mucosal glycoprotein. Well, the auxiliary PVA shows a better sustained-release effect. Fe_3O_4-PVA @SH showed high drug loading levels during the experiment. At the same time, drug release experiments showed that the drug release rate and quantity of Fe_3O_4-PVA@SH reached the release requirements of the 2019 US Pharmacopoeia Aspirin sustained-release tablets. We prepared a targeted magnetically drug carrier with a high potential for drug delivery and prevented the whole body's excess distribution and eliminated its side effects. Our magnetic systems can easily reach the target point by applying an external magnetic field, while the superparamagnetic requires a smaller area than previously published works. When these nanoparticles begin to decompose inside the body, soluble iron is harmful and can be used in the patient with iron-deficiency anemia.

4. Conclusions

In conclusion, we successfully proved that the coupling agent (TIPTS) could be used in biology as a material for improving amphiphilicity and improving the liposolubility of magnetic drugs. Aspirin can be administered orally by loading on a magnetically targeting nanocarrier. The magnetic targeting drug carrier prepared experimentally has an excellent drug loading rate and a stable release for 8 hours. The present work is of interest for opening up enormous opportunities to make full use of magnetic carrier material in drug delivery and other applications, because of their easy availability, cost-effective productivity, and profitable drug release performance.

Acknowledgments

This work was supported by the Fundamental Research Funds in Heilongjiang Provincial Universities (No:135309110).

Disclosure statement

No potential conflict of interest was reported by the authors.

Funding

This work was supported by the Fundamental Research Funds in Heilongjiang Provincial Universities [No:135309110].

ORCID

Yazhen Wang http://orcid.org/0000-0001-9314-5222

References

[1] Giovanni Tosi JT, Duskey JK. Nanoparticles as carriers for drug delivery of macromolecules across the blood-brain barrier. J Expert Opin Drug Delivery. 2020;17(1):23–32.
[2] Kimna C, Lieleg O, et al. Engineering an orchestrated release avalanche from hydrogels using DNA-nanotechnology. J Controlled Release. 2019;28:19–28.
[3] Rajasree S, Edison, Thomas TNJI, et al. Chitosan nanopolymers: an overview of drug delivery against cancer. J Int Biol Macromol. 2019;130:727–736.
[4] Guo-Ying S, Yi-Chen, Cui Y, et al. Terminal deoxynucleotidyl transferase-catalyzed preparation of pH-responsive DNA nanocarriers for tumor-targeted drug delivery and therapy. J ACS Appl Mater Interfaces. 2019;11:14684–14692.
[5] B K L, E C T, S D K. The use of magnetic targeting for drug delivery into cardiac myocytes. J Magn Magn Mater. 2018;473:21–25.
[6] R D J, Gupta P, Garcia E, et al. Nanoparticle based treatment for cardiovascular diseases. J Cardiovasc Hematol Disord Drug Targets. 2018;19:33–44.
[7] Piumi Y, Liyanage SD, Hettiarachchi YZ, et al. Nanoparticle-mediated targeted drug delivery for breast cancer treatment. J Biochimica et Biophysica Acta (BBA). 2019;1871:419–433.
[8] Xiaolei G, Wei, Yaohua Y, et al. cRGD-decorated biodegradable polytyrosine nanoparticles for robust encapsulation and targeted delivery of doxorubicin to colorectal cancer in vivo. J Controlled Release. 2019;301:110–118.
[9] Ali D, Hedayatnasab, Ziba Z, et al. Polyethylene glycol-coated porous magnetic nanoparticles for targeted delivery of chemotherapeutics under magnetic hyperthermia condition. J Int J Hyper. 2019;36:104–114.
[10] Pritam S, Kunda M, Chatterjee S, et al. Targeted delivery of quercetin via pH-responsive zinc oxide nanoparticles for breast cancer therapy. J Mater Sci Eng. 2019;100:129–140.
[11] Patel J, Misra A, Javia A, et al. Targeted delivery of monoclonal antibody conjugated docetaxel loaded

PLGA nanoparticles into EGFR Overexpressed lung tumor cells. J Microencapsulation. 2018;35:204–217.
[12] Firdos A, Akhtar, Khan S, et al. Targeted delivery of poly (methyl methacrylate) particles in colon cancer cells selectively attenuates cancer cell proliferation. J Artificial Cells Nanomed Biotechnol. 2019;47:1533–1542.
[13] Xuan S, Wang F, Lai JMY, et al. Synthesis of biocompatible, mesoporous Fe_3O_4 Nano/microspheres with large surface area for magnetic resonance imaging and therapeutic applications. J ACS Appl Mater Interfaces. 2011;3:237–244.
[14] Xu L, Qiu L, Sheng Y, et al. Biodegradable pH-responsive hydrogels for controlled dual-drug release. J Mater Chem B. 2017;6:510–517.
[15] Thanh VM, Nguyen TH, Tran TV, et al. Low systemic toxicity nanocarriers fabricated from heparin-mPEG and PAMAM dendrimers for controlled drug release. J Mater Sci Eng C Mater Biol Appl. 2018;82:291–298.
[16] Li Y, Jin J, Wang D, et al. Coordination-responsive drug release inside gold nanorod@metal-organic framework core-shell nanostructures for near-infrared-induced synergistic chemo-photothermal therapy. J Nano Res. 2018;16:3294–3305.
[17] Ling W, Wang M, Xiong C, et al. Synthesis, surface modification, and applications of magnetic iron oxide nanoparticles. J Mater Res. 2019;34:1828–1844.
[18] Pillarisetti S, Uthaman S, Huh KM, et al. Multimodal composite iron oxide nanoparticles for biomedical applications. J Tissue Eng Regenerative Med. 2019;16:451–465.
[19] Rasouli E, Basirun WJ, Johan MR, et al. Facile and greener hydrothermal honey-based synthesis of Fe_3O_4/Au core/shell nanoparticles for drug delivery applications. J Cellular Biochem. 2018;120:6624–6631.
[20] Gyergyek S, Makovec D, Jagodič M, et al. Hydrothermal growth of iron oxide NPs with a uniform size distribution for magnetically induced hyperthermia: structural, colloidal and magnetic properties. J Alloys Compd. 2017;694:261–271.
[21] Wang W, Lin J, Xing C, et al. Fe_3O_4 nanoparticle-coated boron nitride nanospheres: synthesis, magnetic property and biocompatibility study. J Ceramics Int. 2017;43:6371–6376.
[22] Peralta ME, Jadhav SA, Magnacca G, et al. Synthesis and in vitro testing of thermoresponsive polymer-grafted core-shell magnetic mesoporous silica nanoparticles for efficient controlled and targeted drug delivery. J Colloid Interface Sci. 2019;544:198–205.
[23] Perera AS, Zhang S, Homer-Vanniasinkam S, et al. Polymer-magnetic composite fibers for remote-controlled drug release. J ACS Appl Mater Interfaces. 2018;10:15524–15531.
[24] Yadavalli T, Ramasamy S, Chandrasekaran G, et al. Dual responsive PNIPAM-chitosan targeted magnetic nanopolymers for targeted drug delivery. J Magn Magn Mater. 2015;380:315–320.
[25] Zhang J, Misra RDK. Magnetic drug-targeting carrier encapsulated with thermosensitive smart polymer: core–shell nanoparticle carrier and drug release response. J Acta Biomaterialia. 2007;3:838–850.
[26] Dong Y, Chen H, Chen C, et al. Polymer-lipid hybrid theranostic nanoparticles co-delivering ultrasmall superparamagnetic iron oxide and paclitaxel for targeted magnetic resonance imaging and therapy in atherosclerotic plaque. J Biomed Nanotechnol. 2016;12:1245–1257.
[27] Nosrati H, Sefidi N, Sharafi A, et al. Bovine Serum Albumin (BSA) coated iron oxide magnetic nanoparticles as biocompatible carriers for curcumin-anticancer drug. J Bioorganic Chem. 2018;76:501–509.
[28] Prerana C, Balaji, Wang Q et al. Biocompatible nanoparticles and vesicular systems in transdermal drug delivery for various skin diseases. J Pharm. 2018;55:49–62.
[29] Yew YP, Shameli K, Miyake M, et al. Green biosynthesis of superparamagnetic magnetite Fe_3O_4 nanoparticles and biomedical applications in targeted anticancer drug delivery system: A review. J Arabian Chem. 2020;13:2287–2308.
[30] Yu J, Zhao F, Gao W, et al. Magnetic reactive oxygen species nanoreactor for switchable magnetic resonance imaging guided cancer therapy based on pH-sensitive Fe_5C_2@Fe_3O_4 nanoparticles. J ACS Nano. 2019;13:10002–10014.
[31] Arriortua OK, Insausti M, Lezama L, et al. RGD-functionalized Fe_3O_4, nanoparticles for magnetic hyperthermia. J Colloids Surf B Biointerfaces. 2018;165 (2018):315–324.
[32] Tao C, Chen T, Liu H, et al. Design of biocompatible Fe_3O_4@MPDA mesoporous core-shell nanospheres for drug delivery. J Microporous Mesoporous Mater. 2019;293:109823.
[33] Tarhan T, Ulu A, Sariçam M, et al. Maltose functionalized magnetic Core/Shell Fe_3O_4@Au nanoparticles for an efficient L-Asparaginase immobilization. J Biol Macromol. 2020;142:443–451.
[34] Masood F. Polymeric nanoparticles for targeted drug delivery system for cancer therapy. J Mater Sci Eng C. 2016;60:569–578.
[35] Alireza H, Irandoust M, Soleimani E, et al. Increasing the anticancer activity of azidothymidine toward the breast cancer via rational design of magnetic drug carrier based on molecular imprinting technology. J Mater Sci Eng C. 2019;103:109771.
[36] Hu X, Wang Y, Zhang L, et al. design of a pH-sensitive magnetic composite hydrogel based on salecan graft copolymer and Fe_3O_4@SiO_2 nanoparticles as drug carrier. J Biol Macromol. 2018;107:1811–1820.
[37] Sargazi G, Afzali D, Mostafavi A, et al. Synthesis of CS/PVA biodegradable composite nanofibers as a microporous material with well controllable procedure through electrospinning. J Polym Environ. 2018;26:1804–1817.
[38] El-Newehy MH, El-Naggar ME, Alotaiby S, et al. Preparation of biocompatible system based on electrospun CMC/PVA nanofibers as controlled release carrier of diclofenac sodium. J Macromol Sci A. 2016;53:566–573.
[39] Engelke L, Winter G, Engert J. Application of water-soluble polyvinyl alcohol-based film patches on laser microporated skin facilitates intradermal macromolecule and nanoparticle delivery. J Euro J Pharm Biopharm. 2018;128:119–130.

[40] Dathathri E, Lal S, Mittal M, et al. Fabrication of low-cost composite polymer-based micro needle patch for transdermal drug delivery. J Appl Nanosci. 2020;10:371–377.
[41] Sha Y, Yun, Sixin-Cui, et al. Chitosan-polyvinyl alcohol nanoscale liquid film-forming system facilitates MRSA-infected wound healing by enhancing antibacterial and antibiofilm properties. J IntNanomed. 2018;13:4987–5002.
[42] Rac V, Lević S, Balanč B, et al. PVA Cryogel as model hydrogel for iontophoretic transdermal drug delivery investigations. Comparison with PAA/PVA and PAA/PVP interpenetrating networks. J Colloids Surf B. 2019;180:441–448.
[43] Piacentini E, Bazzzarelli F, Poerio A, et al. Encapsulation of water-soluble drugs in Poly (vinyl alcohol) (PVA)-microparticles via membrane emulsification: influence of process and formulation parameters on structural and functional properties. J Mater Commun. 2020;24:100067.
[44] Anirudhan TS, Parvathy J, Nair AS, et al. A novel composite matrix based on polymeric micelle and hydrogel as a drug carrier for the controlled release of dual drugs. J Carbohydr Polym. 2016;136:1118–1127.
[45] Yang W, Fortunati E, Bertoglio F, et al. Polyvinyl alcohol/chitosan hydrogels with enhanced antioxidant and antibacterial properties induced by lignin nanoparticles. J Carbohydrate Polym. 2018;181:275–284.
[46] Nguyen CN, Nguyen TTT, Nguyen HT, et al. Nanostructured lipid carriers to enhance transdermal delivery and efficacy of diclofenac. J Drug Delivery Transl Res. 2017;7:664–673.
[47] El-Naggar A, Senna, Wahab MM, et al. Radiation synthesis and drug delivery properties of interpenetrating networks (IPNs) based on poly(vinyl alcohol)/methylcellulose blend hydrogels. J Biol Macromol. 2017;102:1045–1051.
[48] George L, Bavya MC, Rohan KV, et al. A therapeutic polyelectrolyte–vitamin C nanoparticulate system in a polyvinyl alcohol–alginate hydrogel: an approach to treat skin and soft tissue infection caused by, Staphylococcus aureus. J Colloids Surf B Biointerfaces. 2017;160:315–324.
[49] Shamloo A, Sarmadi M, Aghababaie Z, et al. Accelerated full-thickness wound healing via sustained bFGF delivery based on a PVA/chitosan/gelatin hydrogel incorporating PCL microspheres. J Int J Pharm. 2018;537:278–289.
[50] Yang CY, Song B, Ao Y, et al. biocompatibility of amphiphilic diblock copolypeptide hydrogels in the central nervous system. J Biomater. 2009;30:2881–2898.
[51] Patel A, Gaharwar AK, Iviglia G, et al. Highly elastomeric poly(glycerol sebacate)-co-poly(ethylene glycol) amphiphilic block copolymers. J Biomater. 2013;34:3970–3983.
[52] Duggan S, Cummins W, O' Donovan O, et al. Thiolated polymers as mucoadhesive drug delivery systems. J Euro J Pharm Sci. 2017;100:64–78.
[53] Suchaoin W, De Sousa IP, Netsomboon K, et al. Mucoadhesive polymers: synthesis and in vitro characterization of thiolated Poly (vinyl alcohol). J Int J Pharm. 2016;503:141–149.
[54] Shih H, H Y L, Lin CC. Improving gelation efficiency and cytocompatibility of visible light polymerized thiol-norbornene hydrogels via addition of soluble tyrosine. J Biomater Sci. 2017;5:589–599.
[55] Zhaoyang C, Sun, Qian Q, et al. Highly sensitive detection of cysteine over glutathione and homo-cysteine: new insight into the Michael addition of mercapto group to maleimide. J Biosensors Bioelectron. 2017;91:553–559.
[56] Xue-ying W, Ya-zhen W, Yu-tao D, et al. Preparation and thermal decomposition kinetics of novel silane coupling agent with Mercapto Group. J Nanomater. 2019;10:1–9.
[57] Weitz JI, Lensing AWA, Prins MH, et al. Rivaroxaban or aspirin for extended treatment of venous thromboembolism. J New Eng J Med. 2017;376:1211–1222.
[58] Ornelas A, Zacharias-Millward N, Menter DG, et al. Beyond COX-1: the effects of Aspirin on platelet biology and potential mechanisms of chemoprevention. J Cancer Metastasis Rev. 2017;36:289–303.
[59] Lucotti S, Cerutti C, Soyer M, et al. Abstract 4196: Aspirin inhibits metastasis in the intravascular phase through the blockade of COX-1-TXA2 pathway in platelets. J Cancer Research. 2018;78:4198–4206.
[60] Lee J, Jeong L, Jung E, et al. Thrombus targeting aspirin particles for near infrared imaging and on-demand therapy of thrombotic vascular diseases. J Controlled Release. 2019;304:164–172.
[61] Gang T, Wang, Yejing Y, et al. Design and performance of sericin/poly(vinyl alcohol) hydrogel as a drug delivery carrier for potential wound dressing application. J Mater Sci Eng C Mater Biol Appl. 2019;101:341–351.
[62] Wu H, Cheng K, He Y, et al. Fe_3O_4-based multifunctional nanospheres for amplified magnetic targeting photothermal therapy and fenton reaction. J ACS Biomater Sci Eng. 2018;7:1–46.
[63] Zhou L, Benzhao H, Zhang F, et al. Facile one-pot synthesis of iron oxide nanoparticles cross-linked magnetic Poly(vinyl alcohol) gel beads for drug delivery. J ACS Appl Mater Interfaces. 2012;4:192–199.
[64] W Q H, Zettl A. Coating single-walled carbon nanotubes with tin oxide. J Nano Letters. 2003;3:681–683.
[65] Venkateswarlu S, Lee D, Yoon M. Bioinspired 2D-carbon flakes and Fe_3O_4 nanoparticles composite for arsenite removal. J ACS Appl Mater Interfaces. 2016;8:23876–23885.